Heliostat structural optimization: A study of wind load effects with CFD-FEM methods

Leticia Aldaz, Michael Burisch, Fritz Zaversky, Marcelino Sánchez, Cristóbal Villasante, and David Olasolo

Citation: AIP Conference Proceedings **2033**, 210001 (2018); doi: 10.1063/1.5067203
View online: https://doi.org/10.1063/1.5067203
View Table of Contents: http://aip.scitation.org/toc/apc/2033/1
Published by the American Institute of Physics

Heliostat Structural Optimization: a Study of Wind Load Effects with CFD-FEM Methods

Leticia Aldaz[1, a)], Michael Burisch[1], Fritz Zaversky[1], Marcelino Sánchez[1], Cristóbal Villasante[2] and David Olasolo[2]

[1]*CENER(National Renewable Energy Centre of Spain), Solar Thermal Energy Department: Adress; c/Ciudad de la Innovación 7, Sarriguren(Navarra), Spain; Tel: +34948252800*
[2]*IK4-TEKNIKER Parque Tecnológico, C/Iñaki Goenaga,5 Eibar (Guipuzkoa), Spain.*

[a)] Corresponding author: laldaz@cener.com

Abstract. In solar power tower plants, heliostat mirrors reflect the sunlight onto the receiver. The mirrors are supported by the facet structure and when it is deformed, the mirror quality is affected (the sunlight is reflected with less accuracy). For this reason, the facet heliostat stiffness has a direct impact on the final plant efficiency. In order to optimize heliostat facet design and thus reduce costs in solar power tower plants, this work proposes a numerical study of facet deformations due to wind and gravity loads. Calculating those deformations via numerical models helps to improve the facet structure that supports the mirror and, thus, achieve an accurate performance. The main objective of the simulations proposed here is to obtain high optical performance maintaining material costs. Computational Fluid Dynamic (CFD) numerical methods are utilized to calculate the pressure loads due to wind velocity on heliostat surface. In a second step a Finite Element Analysis (FEA) is carried out taking into account those wind loads and the gravity force. CFD-FEA methods allow calculating root mean square error of surface rotations (RMS-error) due to wind and gravity force. This study shows that an improvement in optical quality in the facet structure could be achieved; while still maintaining the material needed in the facet structure.

Abbreviations

A Area of heliostat facet (m^2)	F_y Force in y direction (N)
CAPTure Competitive SolAr Power Towers	RMS Root Mean Square
CFD Computational Fluid Dynamics	α Elevation angle (º)
C_{drag} Force coefficient in drag direction	β Azimuth angle (º)
C_{lift} Force coefficient in lift direction	ε Rotation angle of x axis (º)
DOF Degree of freedom	δ Rotation angle of y axis (º)
FEA Finite Element Analysis	γ Rotation angle of z axis (º)
FEM Finite Element Method	ρ Air density (kg/m^3)
F_x Force in x direction (N)	U Air velocity (m/s)

SolarPACES 2017
AIP Conf. Proc. 2033, 210001-1–210001-11; https://doi.org/10.1063/1.5067203
Published by AIP Publishing. 978-0-7354-1757-1/$30.00

INTRODUCTION

Reducing heliostat cost is of high interest due to the amount of investment they represent in solar power tower plants [1]. A significant amount of the costs is due to the price of the material of the supporting structure, which is required to prevent deformations of the heliostat and the facet. Studying wind loads and gravity effects on heliostat facets gives a better understanding of these deformations, allowing potential cost savings by reducing the amount of material needed for the structure. The current study focuses on the facet structure optimization, and although the heliostat supporting structure is taken into account in the simulations, it is not optimized.

As the main load of a heliostat is caused by wind [2], an optimum heliostat facet design depends on the estimation of realistic wind loads. Previous studies examine the wind load effects on heliostat via CFD numerical methods and show that CFD tools can give valuable information and good agreement with experimental results [3 and 4]. Other authors use finite element models to estimate deformations on heliostat structures [5]. This study proposes a major challenge, a combination of both analyses (FEM and CFD) in a fluid structure interaction simulation, where the heliostat facet surface acts as an interface between the air and the heliostat domains, providing a mean to transfer mechanical loads generated by the wind velocity. The CFD-FEM interaction method describes the process of mapping the physical properties resulting from the computational fluid dynamic analysis into the finite element model.

As stated in [6] [7], it is highly recommended to consider dynamic induced wind loads when designing a heliostat. Although, excessive stress cycles due to frequently occurring winds could result in failures related to fatigue due to repeated dynamic excitation, in this study, dynamic structural analysis and structural failure of heliostat from overstressing fatigue design is not addressed. In this study, a static analysis is performed in order to have an overall idea of the structural behavior regarding optical performance. In a further step, a dynamic wind induced analysis as it is explained in [7] would be recommended.

In the framework of CAPTure (Competitive SolAr Power Towers) project [8], fluid structure simulations are performed so as to analyze heliostat facet deformations caused by wind loads and gravity force. Angular deformations affect optical performance, and thus, when they exceed the allowable value of angular deformation, the reflected image is distorted excessively. For this analysis, a minimum root mean square RMS-error of surface angular deformations allowable is defined as design criteria, the RMS- error serves to measure the surface rotations and thus the optical imperfection of the mirror surface. The aim is to optimize the facet structure achieving a low cost and high optical performance.

As a result of this study, an optimized design (facet structure) that takes into account the weight, cost and number of joints of the heliostat structure is obtained. Different initial structures are defined and simulated as starting point; from the rotational results obtained from these analyses the RMS-error is calculated for each structure. The maximum value of facet structure mass is set to 50 kg according to cost design criteria. The number of joints, varied in a range from 18 to 24, is set examining local rotations. Comparing the results of different design proposed an optimization of the facet structure (bars) is done meeting the weight, cost and joint requirements.

SIMULATIONS DESCRIPTION

Geometry Description

The simulation performed is for a single facet heliostat with an area of 8 m^2. The support structure is formed by a series of connected metal bars to which the facet is connected by a series of joints. The process of optimization consists in varying the design (number, location and profile of bars) and the number and position of the joints. The improvements are made following the design criteria: optical performance (minimum angular RMS-error) and low cost configurations (material reduction).

Figure 1 (a) shows the coordinate system used for heliostat drag and lift forces definition extracted from [9], and Fig. 1(b) shows the coordinate system used in the model. The coordinate system x axis of [9] corresponds with the drag force direction which is the z direction in the present CFD-FEM model (see Fig. 1(b)). Lift force direction corresponds with the z axis in [9] and with the y axis in the present model's coordinate system.

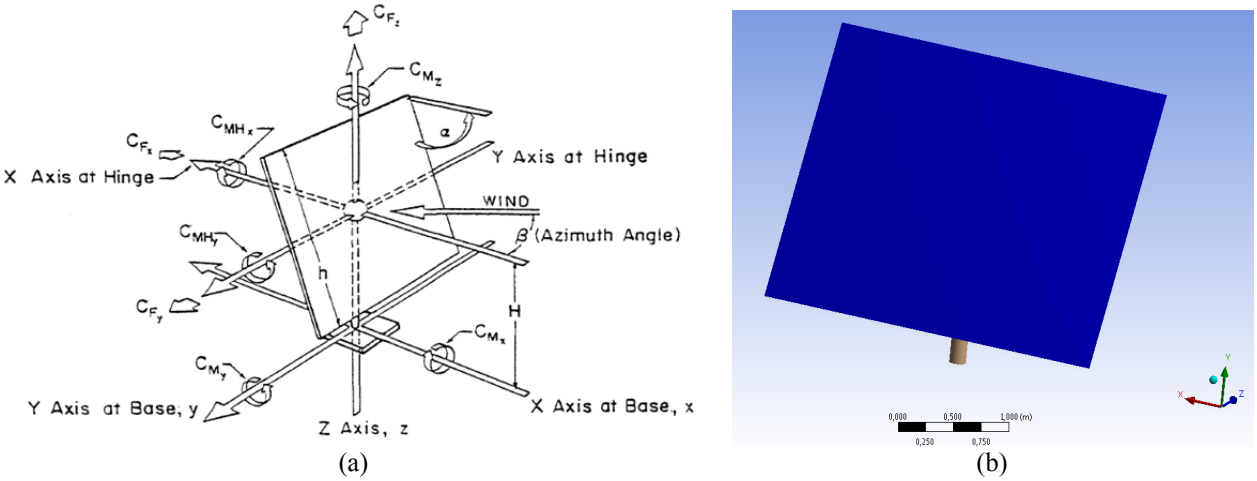

FIGURE 1. (a)Heliostat coordinate system used from [9] and (b) coordinate system for geometry analyzed in the model.

CFD Model Validation

The software used for CFD simulation is ANSYS Fluent. Fluent is used to evaluate the fluid flow around the facet, providing detailed information about the behavior of the fluid flow, in this case, the distribution of wind pressure on the facet.

A realizable k-ε turbulence model with enhanced wall treatment has been chosen for the simulations. k-ε turbulence model is the most common model used in CFD to simulate mean flow characteristics for turbulent flow conditions. In this model the turbulence intensity is taken into account and is defined as the ratio of the root mean square of the velocity fluctuations, to the mean flow velocity. The estimation of the turbulence intensity has been made according to experimental data obtained in [9].CFD results are compared with the results obtained in previous studies [9, 10 and 11] and validated against [10 and 11]. In order to validate the model, simulations for an elevation angle of 0º, 10º, 20º, 30º, 40º, 50º, 60º, 70º, 80º and 90º, azimuth angle of 0º and a wind velocity of 10 m/s are run. Drag (C_{drag}) and lift (C_{lift}) coefficients are calculated according to Equations (1) and (2). These results are compared against the ones obtained by Peterka et al [10] and by Google [11].

$$C_{drag} = \frac{F_{drag}}{\frac{1}{2}\rho U^2 A} \tag{1}$$

$$C_{lift} = \frac{F_{lift}}{\frac{1}{2}\rho U^2 A} \tag{2}$$

Figure 2 shows the comparison between drag and lift coefficients. The drag and lift coefficients due to wind load on heliostat facet are slightly lower in the CFD simulations than in Peterka et al. [10], but higher than in Google [11]. The lift and drag coefficients are calculated to validate the CFD model. For the static analysis the pressures on the surface are imported in the finite element model. A higher value of these coefficients means higher pressure loads on the surface and it can also lead to a heliostat structure oversizing. As Fig. 2 shows, the results are not exactly the same; as through the definition of the model many assumption and simplifications are made, the difference in the results could be caused by many factors. In general, the tendency of ANSYS-Fluent simulations agrees well with the results obtained by Peterka et al. [10].

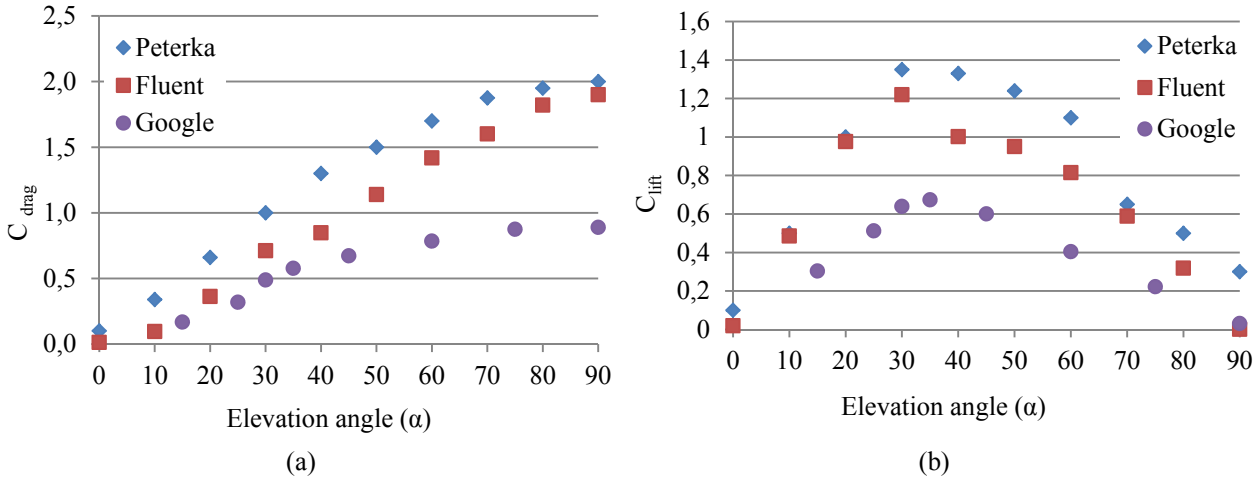

FIGURE 2. (a) Peterka, Google and Fluent drag coefficients comparison (b) Peterka, Google and Fluent lift coefficients comparison

CFD Analysis

The purpose of CFD simulations is to obtain detailed information about fluid flow performance around the heliostat, specifically; the objective is to calculate pressure loads onto the surface due to wind forces in real conditions. When calculating deformations on the facet structure, defining loads properly is of crucial importance.

Therefore, CFD turbulence models for representative cases are simulated. In order to handle the problem, some simplifications and assumptions need to be made. The geometry is composed of one single heliostat with an elevation angle of 60º (α, see Fig. 1(a)). The value has been selected because it is one of the most frequent orientations of a heliostat at latitude of 38º north according to an analysis over the course of a year (see Fig. 3(b)). Different wind conditions are studied. Critical azimuth angles of 0º, 65º and 180º are simulated and wind velocities of 10 m/s and 5m/s are selected according to operational design criteria.

The definition of the problem includes boundary conditions (see Fig. 3 (a)). The control volume of air shown in Fig. 3 (a) is analyzed. A velocity inlet boundary condition is used to define the air flow velocity inlet on the front face. Symmetry condition is applied to lateral and upper walls; this condition can be summarized in a zero normal velocity and a zero normal gradient of all variables at a symmetry plane. The ground is set as wall and a pressure outlet condition is applied to outlet surface.

The domain is discretized into a finite set of control volumes. In the cases analyzed in this article, the CFD code solves equations for conservation of mass and momentum in this set of control volumes. Results of pressure contours on the heliostat facet (see Fig. 4), velocity lines (see Fig. 4) and net force results due to wind loads on the surface for the cases studied (see Table 1) are obtained.

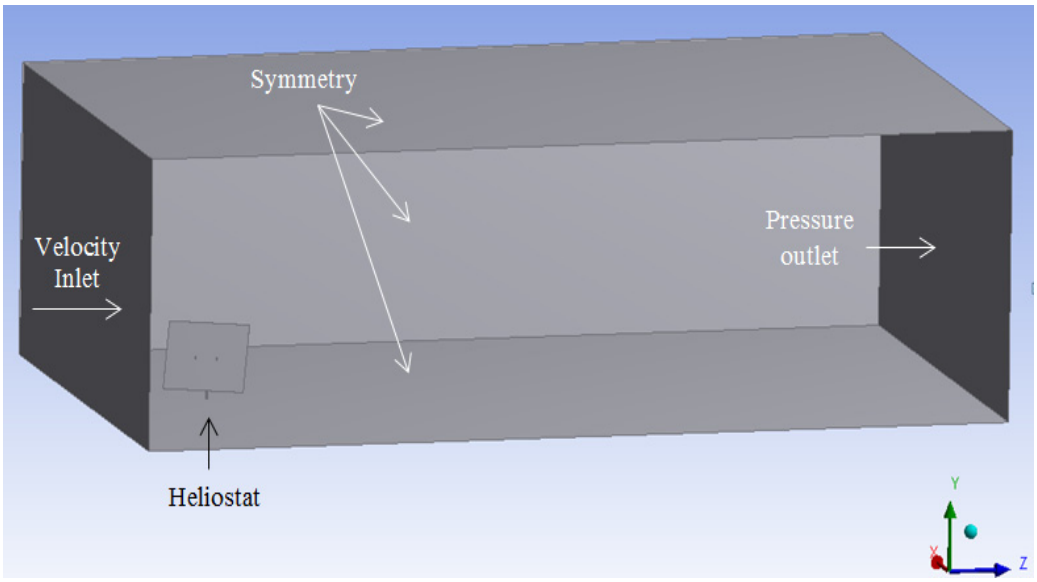

(a)

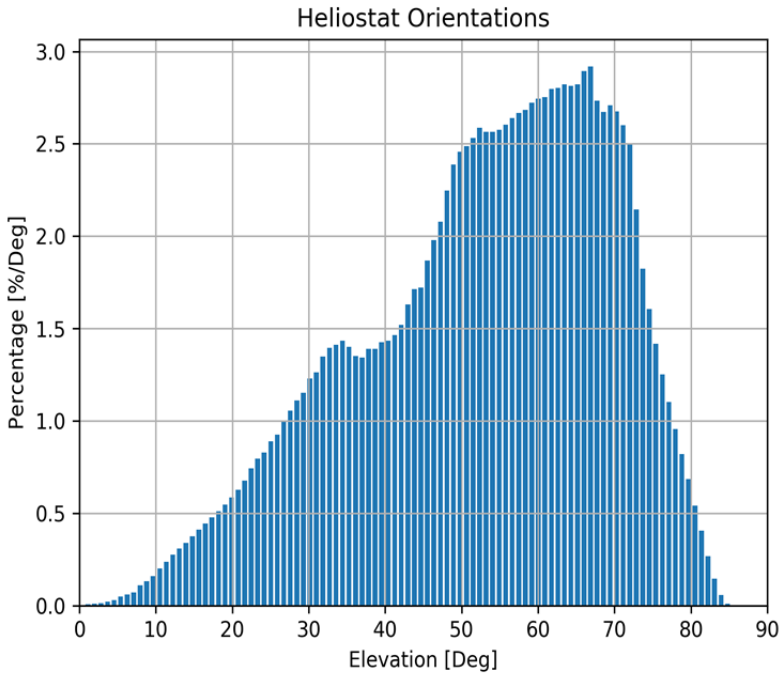

(b)

FIGURE 3. (a) Heliostat elevation orientation over the course of a year (b) boundary conditions in Fluent model

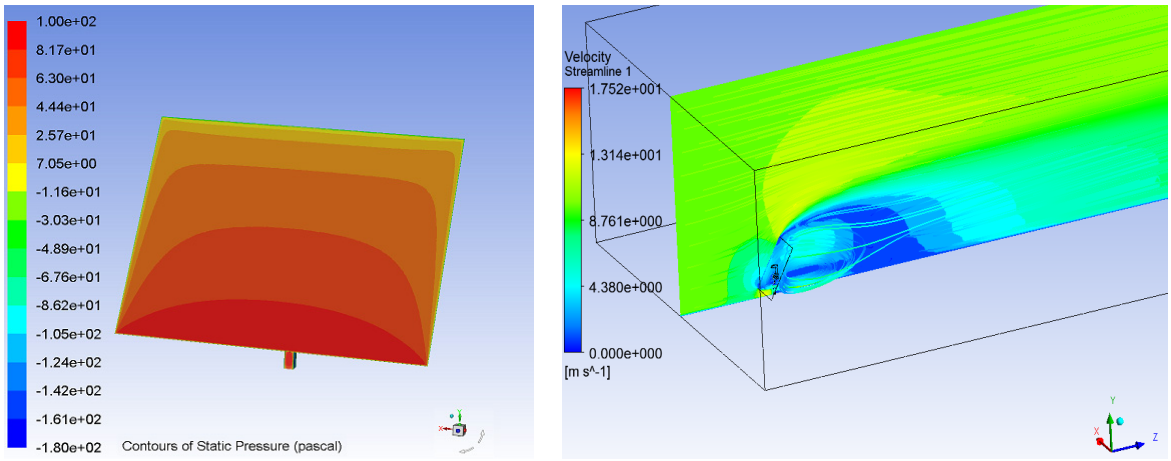

(a)

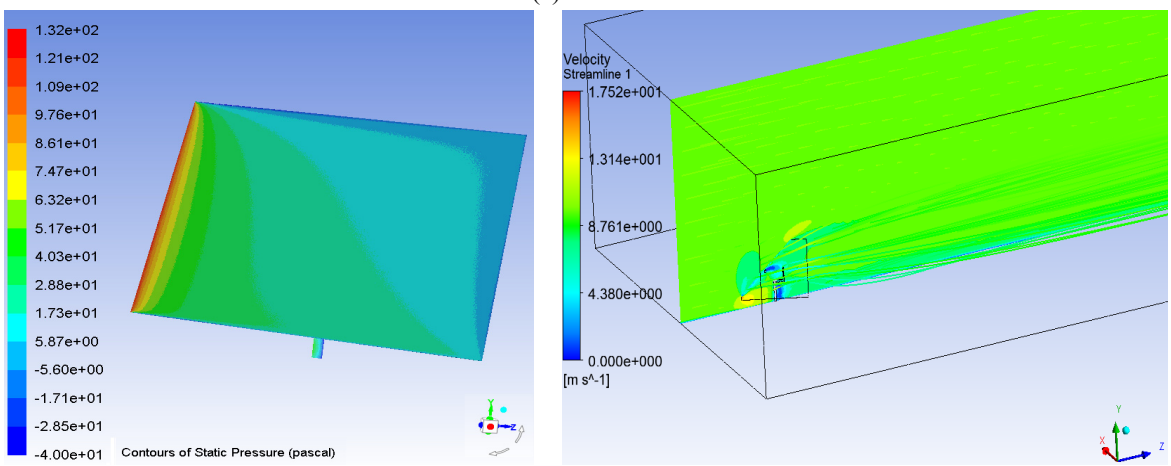

(b)

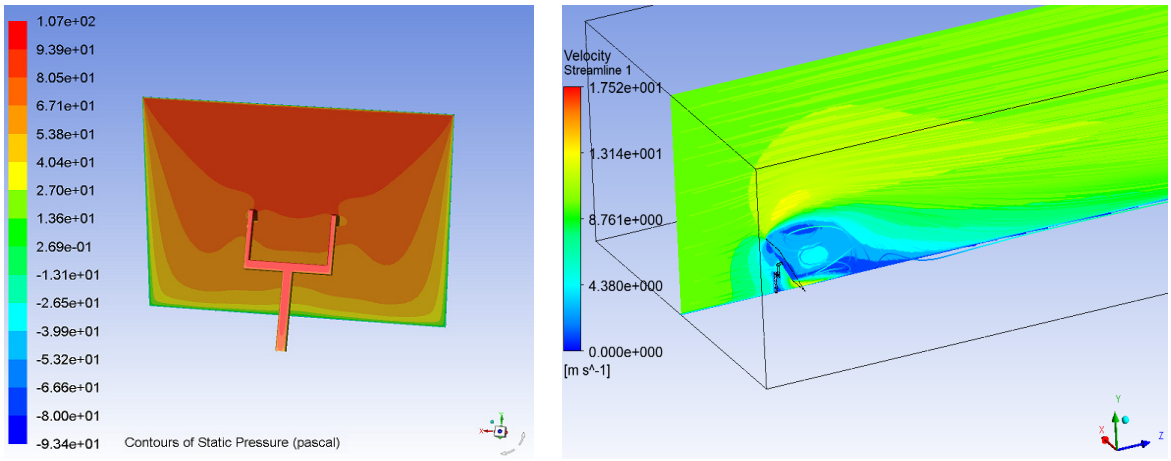

(c)

FIGURE 4. Pressure (Pa) (left), velocity lines (m/s) for a wind velocity of 10 m/s (right), a) Case1, b) Case2 and c) Case3

TABLE 1. Net force results on heliostat surface (N) for a wind velocity of 10 m/s

Case	Elevation angle(º)	Azimuth angle(º)	Fx(N)	Fy(N)	Fz(N)
1	60	0	0	-406	707
2	60	65	405	-258	193
3	60	180	0	460	799

FEM Static Analysis

In order to estimate the deformations caused by this wind load and the weight of the facet structure, a FEM analysis is made. The pressure results obtained in the CFD analyses are transferred into the finite element model. Furthermore, earth gravity effects are included into the model. The solution of the model is calculated in ANSYS Mechanical, giving the deformations of the structure and the facet.

The FEM model consists of 2D elements for modeling the facet and 1D beam elements for modeling the structure (See Fig. 5(a)). Joints between facet structure and mirror are modeled with rigid elements. As load conditions, the pressures obtained from the CFD analysis and gravity force are defined. As the structure is supported in the base of the heliostat, in the model the six degrees of freedom (DOF) are constrained at this point (see Fig. 5(b)). A linear static analysis solution is used to determine nodal displacements.

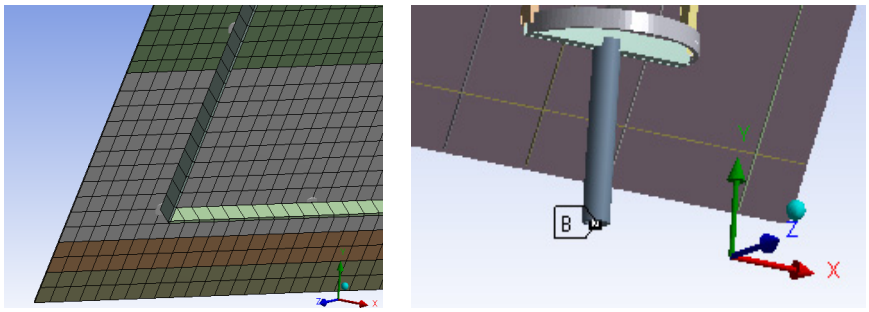

(a) (b)

FIGURE 5. (a) Detail of bars (1D and 2D elements) and joints (b) supporting point constrained (B)**.**

In order to have an overall idea of the optical error, the total rotation between normal vectors of the facet surface before and after deformation is calculated for each node using quaternions rotations. A rotation through an angle of θ around the axis defined by a unit vector ($\vec{u} = u_x i + u_y j + u_z k$) can be represented by a quaternion. This can be done using an extension of Euler´s formula:

$$\mathrm{q} = e^{\frac{\theta}{2}(u_x i + u_y j + u_z k)} = cos\frac{\theta}{2} + (u_x i + u_y j + u_z k) sin\frac{\theta}{2} \tag{1}$$

It can be shown that the general rotation of an angle ε around the x axis, a rotation of an angle γ around the y axis and a rotation of an angle δ around the z axis can be represented by:

$$q_x = \begin{pmatrix} cos\frac{\varepsilon}{2} \\ sin\frac{\varepsilon}{2} \\ 0 \\ 0 \end{pmatrix}; q_y = \begin{pmatrix} cos\frac{\gamma}{2} \\ 0 \\ sin\frac{\gamma}{2} \\ 0 \end{pmatrix}; q_z = \begin{pmatrix} cos\frac{\delta}{2} \\ 0 \\ 0 \\ sin\frac{\delta}{2} \end{pmatrix} \tag{2}$$

x and y rotation quaternions can be combined into one equivalent z quaternion by the relation $q_z=q_x q_y$:

$$\begin{pmatrix} cos\frac{\varepsilon}{2} \\ sin\frac{\varepsilon}{2} \\ 0 \\ 0 \end{pmatrix} \begin{pmatrix} cos\frac{\gamma}{2} \\ 0 \\ sin\frac{\gamma}{2} \\ 0 \end{pmatrix} = \begin{pmatrix} cos\frac{\rho}{2} \\ 0 \\ 0 \\ sin\frac{\rho}{2} \end{pmatrix} \tag{3}$$

$$\text{then} \begin{pmatrix} cos\frac{\varepsilon}{2}cos\frac{\gamma}{2} \\ sin\frac{\varepsilon}{2}cos\frac{\gamma}{2} \\ sin\frac{\gamma}{2}cos\frac{\varepsilon}{2} \\ -sin\frac{\gamma}{2}sin\frac{\varepsilon}{2} \end{pmatrix} = \begin{pmatrix} cos\frac{\rho}{2} \\ 0 \\ 0 \\ sin\frac{\rho}{2} \end{pmatrix} \tag{4}$$

This can be simplified in next equation:

$$cos\frac{\varepsilon}{2}cos\frac{\gamma}{2} = cos\frac{\delta}{2} \tag{5}$$

$$\text{then } \delta = 2cos^{-1}(cos\frac{\varepsilon}{2}cos\frac{\gamma}{2}) \tag{6}$$

Thus, the rotations in x and y represented in a coordinate system aligned with the facet mirror are extracted and total rotations are calculated according to equation (6). The z axis is perpendicular to the surface, thus rotations in z do not cause angular surface deformations. Where ε is x rotation and γ is y rotation in radians according to the coordinate system shown in Fig. 7.

The RMS-error is calculated for the lower 95% range of the node results to exclude high values that can distort the final RMS value.

Initially, three configurations A (Fig. 6 (a)), B (Fig. 6 (b)) and C (Fig. 6(c)) are analyzed for three different cases: Case1 (azimuth angle of 0º), Case2 (azimuth angle of 65º) and Case3 (azimuth angle of 180º). The RMS-error is calculated for different numbers and location of joints. From these simulations, the optimum results are selected according to their lowest RMS-error values and shown in Table 2.

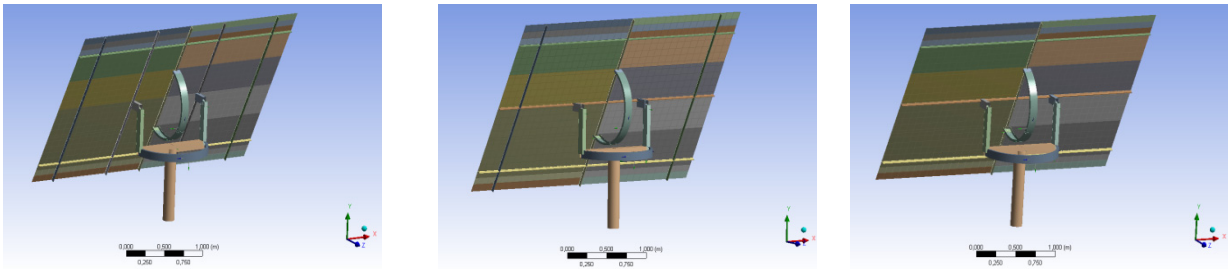

(a) (b) (c)

FIGURE 6. Different bar location studied, (a) A, (b) B and (c) C

Since configuration B shows the lowest values of RMS-error, even though it is not the lightest, it is selected for a second optimization loop. Furthermore, in this second optimization stage, Case2 is selected as critical because, in general, it has higher values of rotations. The second optimization mainly consists of varying the facet structure beam section to see the impact in the final results. Fig. 8 summarizes the dimensions and sizes of different bar section models. Table 3 and Fig. 9 show the results of RMS-error of this second set of simulations.

Results and Discussion

Once the methodology for calculating RMS-error due to wind and gravity forces is defined, the process of improvement and optimization can be focused on different objectives. In this study, a maximum weight allowed by

the facet structure is defined as design criteria; this value is set to 50 kg. Following this target an improvement of optical RMS-error caused by angular deformations is achieved. When improving optical RMS-error, facet mass structure can be increased, for that reason the maximum mass allowed is limited. Then, defining a maximum weight allowed, the study tries to find a good balance between both parameters, RMS-error and facet weight.

Three different heliostat facet configurations that meet the mass requirements are chosen as optimization starting points (Fig. 6). The RMS-error results for these configurations are listed in Table 2 and the rotation values in rad for each node with the deformed structure (exaggerated) for configuration B are plotted in Fig. 7. According to Table 2, the structure that has the lowest RMS-error value for Case1 is B, for Case2 is B and for Case3 is C. Case3 is not the most critical, because the wind impacts on the rear surface of the facet, and it seems that the deformations due to the wind loads are compensated with deformations due to the gravity forces. Hence, configuration B is selected for continuation with the optimization procedure.

TABLE 2. RMS-error values for different cases and structures

Configuration	Number of joints	Facet structure mass(kg)	Case1		Case2		Case3	
			10 m/s	5 m/s	10 m/s	5 m/s	10 m/s	5 m/s
A	21	47	6	3.5	5.7	2.53	3.6	2.1
B	24	43	3.7	2.2	4.3	2.1	4	2.2
C	21	30	4.1	2.3	12.2	3.46	3.3	1.5

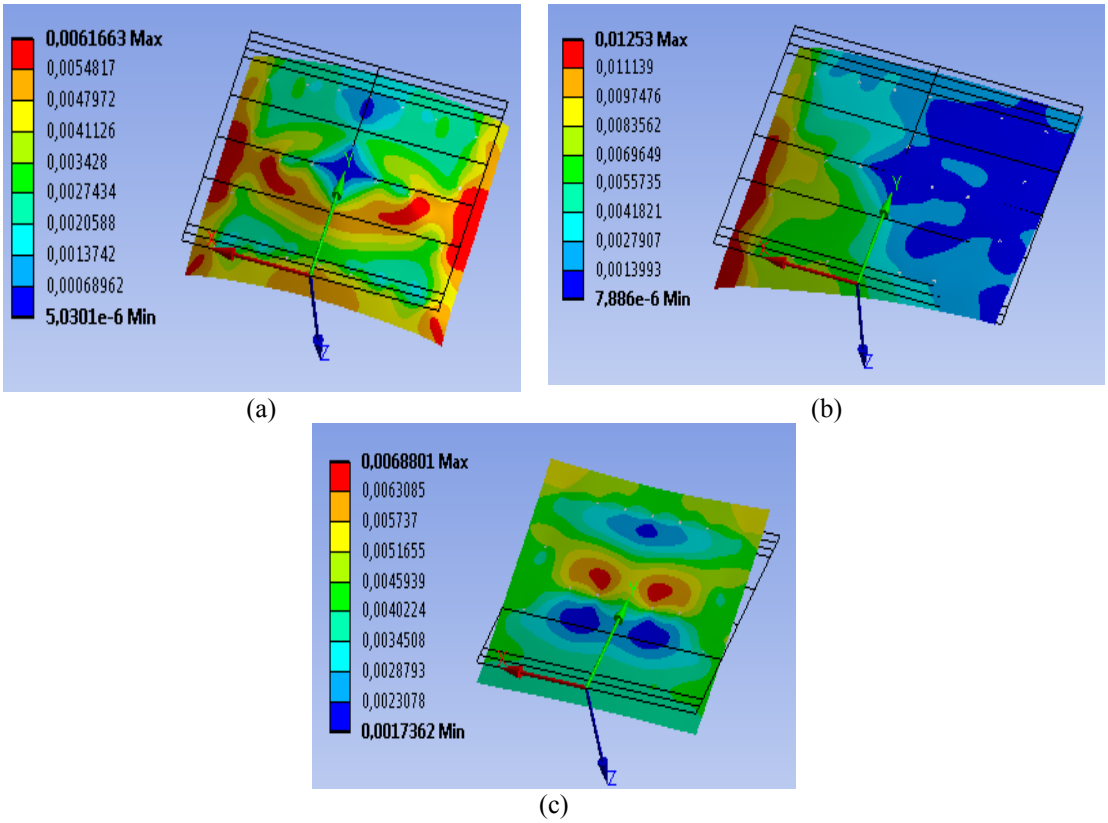

FIGURE 7. Rotation values plot in rad for each node on B deformed structure (undeformed facet is represented in wireframe) (a) Case1, (b) Case2 and (c) Case3.

Starting from configuration B, a second stage of facet structure improvement is done varying the beam sections, Fig. 8 shows the beam sections tested. The section represented in Fig. 8 (b) is the section used for previous

simulations. The deflection of a beam depends on its cross sectional shape. For this reason, beam section is modified in dimensions (from Fig. 8(b) to Fig. 8(c)) and shape (from Fig. 8(c) to Fig. 8(d)) in order to increase the moment of inertia in the direction of main deformations (see Fig. 8(a)).

From this new set of simulations, four new configurations are simulated and analyzed. All the configurations corresponds to B facet structure, B_1 has the Fig. 8 (b) beam section for the facet structure bars, B_2 has the Fig. 8(c) , B_3 has the Fig. 8(d) and B_4 has the Fig. 8(d) beam section and the number of joints is reduced from 24 to 21.

The values of RMS-error calculated with the nodal rotation results are summarized in Table 3 and represented in Fig. 9 and Fig. 10. From these results it can be concluded that the RMS-error value can be reduced and thus the optical quality can be optimized without increasing the material cost. For the initial configuration B and Case2 the RMS-error is reduced from 4.3 to 1.9 mrad for a velocity of 10 m/s and from 2.1 to 0.94 mrad for a velocity of 5 m/s (see Table 2 and Table 3).

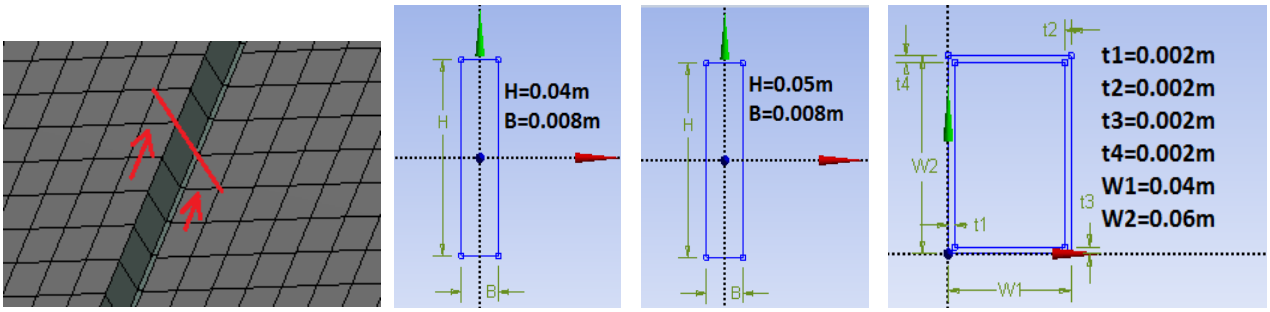

(a) (b) (c) (d)

FIGURE 8. (a) Beam section (b) B_1 dimensions, (c) B_2 dimensions, (d) B_3 and B_4 dimensions

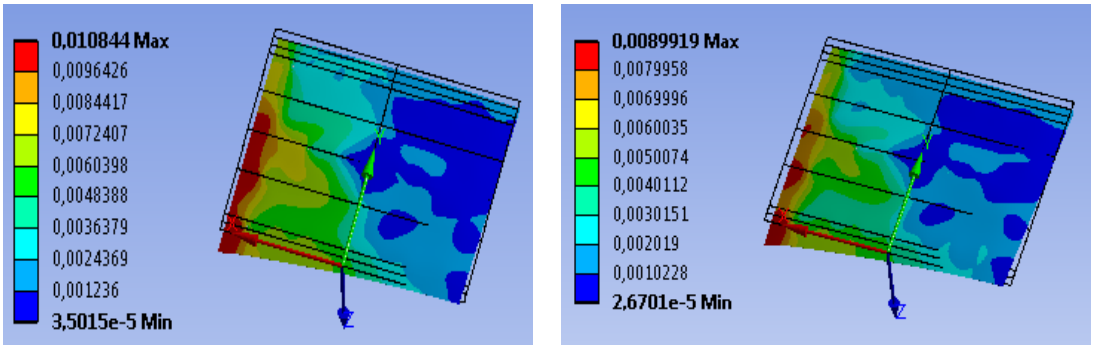

(a) (b)

FIGURE 9. RMS-error plots for deformed structures (a) B_1 and (b) B_2

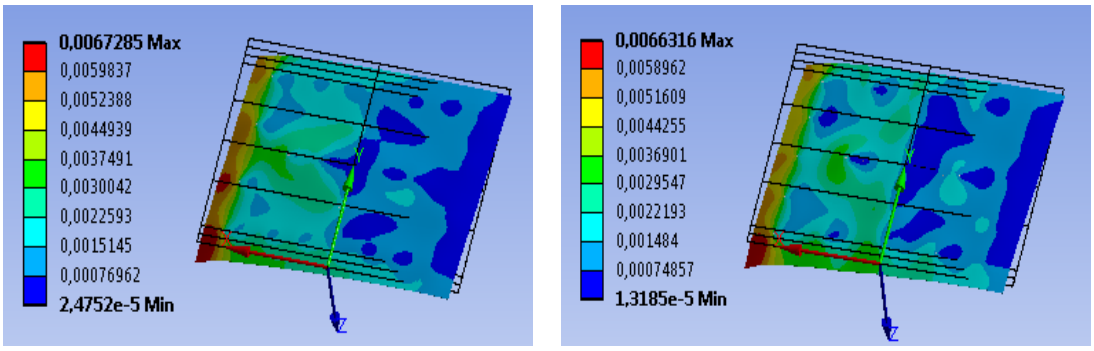

(c) (d)

FIGURE 10. RMS-error plots for deformed structures (a) B_3 and (b) B_4

TABLE 3. Optimization of B configuration by changing the beam section and number of joints

Configuration	Number of joints	Facet structure mass(kg)	RMS-error values (mrad) calculated with nodal rotations of the mirror for Case2	
			10 m/s	5 m/s
B_1	24	34	4.3	1.87
B_2	24	42	2.8	1.39
B_3	24	41	1.9	0.94
B_4	21	41	1.9	0.96

CONCLUSIONS

In order to optimize the optical performance by not increasing the amount of material and thus cost, a computational fluid dynamic (CFD) analysis and a finite element analysis (FEA) are performed. Pressure contours on the mirror surface caused by the wind are calculated with a CFD analysis, and these results are mapped onto a finite element model (FEM) where the static structural behavior and deformations caused by the wind loads and the gravitational forces due to the weight of the reflective surface are analyzed. The results obtained in this study demonstrate that an optimization of the structure is possible utilizing CFD and FEM techniques. These methods are a powerful tool to predict wind load effects on heliostat, and hence help optimizing the heliostat design. This study proves that, for the cases analyzed, a RMS-error reduction of up to 40 % (from 4.3 mrad to 1.9 mrad) in the facet structure could be achieved, without increasing the facet weight, and consequently maintaining the material costs target. As a further step, a dynamic structural and fatigue analysis would be recommended in order to avoid structural failure of the heliostat over its lifetime.

ACKNOWLEDGMENTS

This work has received funding from the European Union's Horizon 2020 research and innovation program under the grant agreement No 640905 [6].

REFERENCES

1. G. J. Kolb, C. K. Ho, T.R. Mancini and J. A. Gary, "Power tower technology roadmap and cost reduction plan" in SAND2011-2419, Sandia National Laboratories Albuquerque, NM7, (2011).
2. A. Pfahl, A. Brucks, and C. Holze, "Wind load reduction for light-weight heliostats" in Energy Procedia, 49, pp. 193-200, (2014).
3. P. E. Poulain, K. Craig and J. P. Meyer, "Influence of the Gap Size on the Wind Loading on Heliostats" in AIP Conference Proceedings 1734, pp. 1-9, (2016).
4. C. K. Ho, "Computational fluid dynamics for concentrating solar power systems" in Wiley Interdisciplinary Reviews: Energy and Enviroment 3, pp 290-300, (2013).
5. L. Amsbeck, R. Buck, A. Pfahl and R. Uhlig, "Optical performance and weight estimation of a heliostat with ganged facets" in Journal of Solar Energy Engineering, 130(1), 011010, (2007).
6. B. Gong, Z. Li, Z. Wang and Y. Wang, " Wind Induced Dynamic Response of Heliostat" in Renewable Energy, 38(1), pp. 206-213, (2012)
7. R. Rebolo, J. Lata and J. Vazquez , "Design of Heliostats Under Extreme and Fatigue Wind Loads" in Proceedings SolarPACES, Granada, (2011).
8. CENER, Horizon 2020 Research Project CAPTure - Competitive SolAr Power Towers - Grant Agreement Number 640905, www.capture-solar-energy.eu, (2015).
9. M. Burisch, I. Santana, M. Sánchez, C. Villasante and E. Olabarrieta, "Experimental Validation of Theoretical Heliostat Wind Loads" in Energy Procedia, 69, pp.50-59, (2015).
10. J. A. Peterka and R. G. Derickson, " Wind load design methods for ground-based heliostats and parabolic dish collectors" in SAND-92-7009, Sandia National Laboratories, Albuquerque, NM, (1992).
11. Google, "RE<C: Heliostat Wind Tunnel Experiments" (2012), Available from https://www.google.org/pdfs/google_heliostat_wind_tunnel.pdf